Transparent Power-Generating Windows Based on Solar-Thermal-Electric Conversion

Fang, Y., Zhang, Q., Huang, A., Ai, X., Liao, J., Song, Q., Reith, H., Cao, X., Schierning, G., Nielsch, K., Bai, S. & Chen, L.

Original citation:
Fang, Y, Zhang, Q, Huang, A, Ai, X, Liao, J, Song, Q, Reith, H, Cao, X, Schierning, G, Nielsch, K, Bai, S & Chen, L 2021, 'Transparent Power-Generating Windows Based on Solar-Thermal-Electric Conversion', Advanced Energy Materials, vol. 11, no. 30, 2101213.
https://dx.doi.org/10.1002/aenm.202101213

DOI 10.1002/aenm.202101213
ISSN 1614-6832
ESSN 1614-6840

Publisher: Wiley

ADVANCED ENERGY MATERIALS
www.advenergymat.de

Transparent Power-Generating Windows Based on Solar-Thermal-Electric Conversion

Qihao Zhang, Aibin Huang, Xin Ai, Jincheng Liao, Qingfeng Song, Heiko Reith, Xun Cao, Yueping Fang, Gabi Schierning,* Kornelius Nielsch,* Shengqiang Bai,* and Lidong Chen*

Integrating transparent solar-harvesting systems into windows can provide renewable on-site energy supply without altering building aesthetics or imposing further design constraints. Transparent photovoltaics have shown great potential, but the increased transparency comes at the expense of reduced power-conversion efficiency. Here, a new technology that overcomes this limitation by combining solar-thermal-electric conversion with a material's wavelength-selective absorption is presented. A wavelength-selective film consisting of $Cs_{0.33}WO_3$ and resin facilitates high visible-light transmittance (up to 88%) and outstanding ultraviolet and infrared absorbance, thereby converting absorbed light into heat without sacrificing transparency. A prototype that couples the film with thermoelectric power generation produces an extraordinary output voltage of ≈4 V within an area of 0.01 m^2 exposed to sunshine. Further optimization design and experimental verification demonstrate high conversion efficiency comparable to state-of-the-art transparent photovoltaics, enriching the library of on-site energy-saving and transparent power generation.

1. Introduction

The urgent goals of tackling climate change and securing sustainable energy sources have triggered the search for innovative and economically attractive means of harnessing solar energy. Transparent power-generating windows (TPGWs), which convert sunlight into electricity, can be an attractive complement to roof-top solar panels, ensuring electricity generation to be an integral part of buildings or automobiles.[1–3] The total area of building glass in China alone is conservatively estimated to be greater than 15 billion m^2.[4] Assuming a module power-conversion efficiency to be 5%, the total potential of window-mounted power-generating systems could reach up to 800 TWh yr^{-1}, which may meet 80% of the total residential

Dr. Q. H. Zhang, Dr. A. B. Huang, Prof. J. C. Liao, Dr. Q. F. Song, Prof. X. Cao, Prof. S. Q. Bai, Prof. L. D. Chen
State Key Laboratory of High Performance Ceramics and Superfine Microstructure
Shanghai Institute of Ceramics
Chinese Academy of Sciences
Shanghai 200050, China
E-mail: cxun@mail.sic.ac.cn; bsq@mail.sic.ac.cn

Dr. Q. H. Zhang, Dr. H. Reith, Prof. G. Schierning, Prof. K. Nielsch
Institute for Metallic Materials
Leibniz Institute for Solid State and Materials Research Dresden (IFW Dresden)
01069 Dresden, Germany
E-mail: gschierning@physik.uni-bielefeld.de; k.nielsch@ifw-dresden.de

Dr. Q. H. Zhang, Dr. A. B. Huang, Prof. X. Cao, Prof. S. Q. Bai, Prof. L. D. Chen
Center of Materials Science and Optoelectronics Engineering
University of Chinese Academy of Sciences
Beijing 100049, China

The ORCID identification number(s) for the author(s) of this article can be found under https://doi.org/10.1002/aenm.202101213.

DOI: 10.1002/aenm.202101213

X. Ai
State Key Laboratory for Modification of Chemical Fibers and Polymer Materials, College of Materials Science and Engineering
Donghua University
Shanghai 201620, China

Prof. Y. P. Fang
School of Energy
Construction and Environment
Coventry University
Coventry CV1 5FB, UK

Prof. G. Schierning
Experimentalphysik
Fakultät für Physik
Universität Bielefeld
Universitätsstr. 25 (D2, Raum 217), 33615 Bielefeld, Germany

Prof. K. Nielsch
Institute of Materials Science
Dresden University of Technology
01062 Dresden, Germany

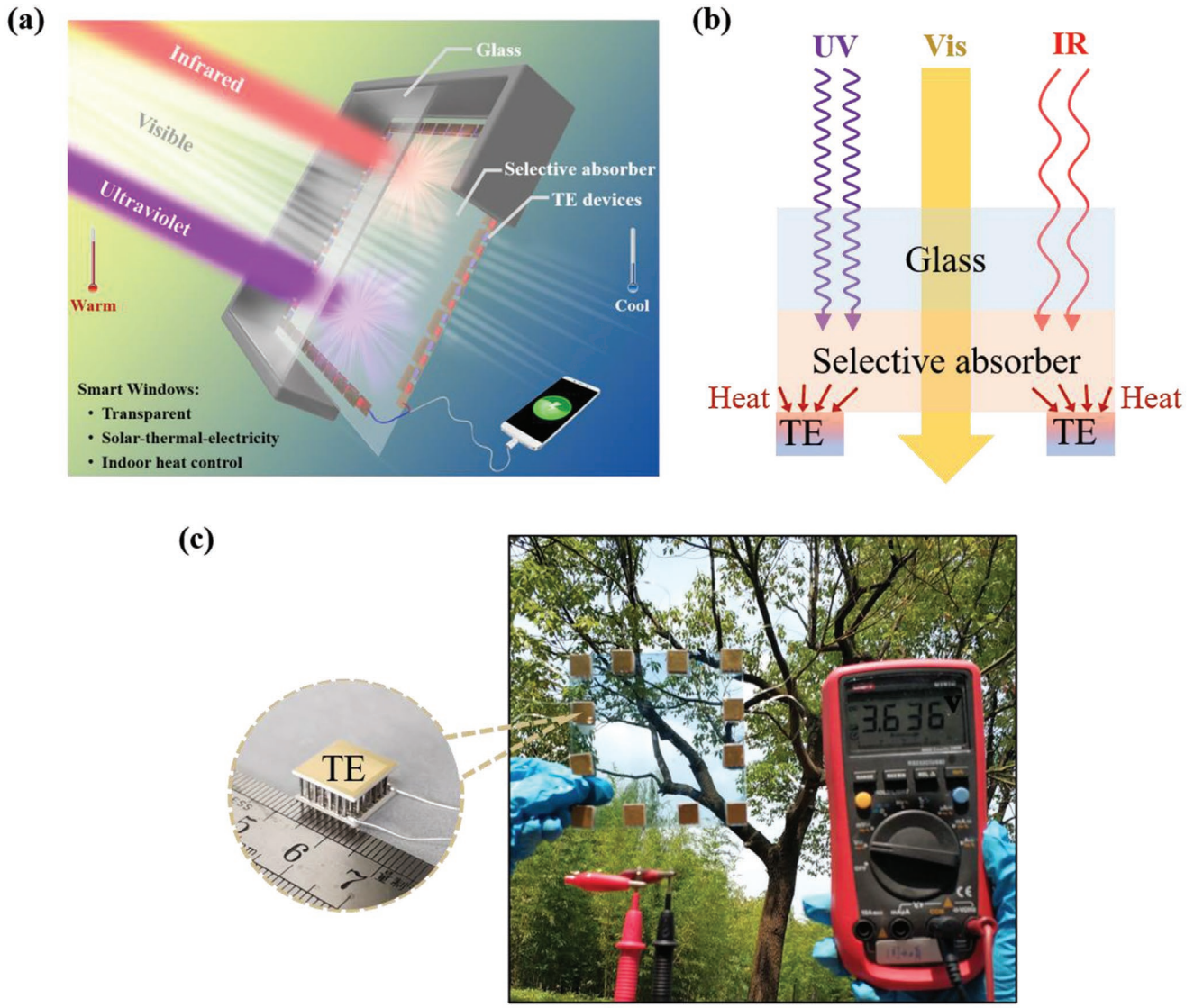

Figure 1. Transparent power-generating windows based on solar-thermal-electric conversion. a) Schematic illustration of the proposed transparent power-generating window architecture and working process. b) Working principle of transparent power generation windows based on wavelength-selective STE in this work. c) Proof-of-concept demonstration of the power-generating performance of a typical solar-thermal-electric power-generating glass containing 12 Bi_2Te_3-based thermoelectric modules in series. A voltage of 3.636 V was obtained by harvesting sunlight in the outdoors at an ambient temperature of ≈20 °C (22 July 2020, Shanghai, China).

electricity demand in China.[1,5] Widespread use of TPGW does not require additional land, reduces building/automobile energy consumption, and provides abundant on-site energy without energy losses on the electricity transmission lines.

Transparent photovoltaic (TPV) technology can be integrated with building and automobile glasses and is thus a promising candidate for use in TPGW.[6–9] However, increased transparency in TPV devices often comes at the expense of power-conversion efficiency. For example, ultrathin perovskite solar cells can yield a high efficiency of 13.6%, but the average visible transmittance is only 7% and such cells should be referred to as semitransparent.[10] Theoretically, the wavelength-selective TPV can optimize the efficiency and transparency simultaneously, however, up to now the experimental results are still far below the theoretical Shockley-Queisser limit.[1] For example, an average visible transmittance of up to 88% has been demonstrated in the transparent luminescent solar concentrators, but the power-conversion efficiency is lower than 0.5%.[11] Although multijunction cells could offer the best possible combination of transparency and efficiency, the resulting infrared thermal load may lead to poor reliability and even reduced conversion efficiency.[12] Moreover, TPV devices are also limited by the problems such as excitonic limitations, optical losses, resistive losses, and air sensitivity.[1]

Solar-thermal-electric (STE) conversion is another effective strategy for harvesting solar energy and converting it into electricity.[13–19] This technique combines photothermal and thermoelectric effects, whereby the temperature difference induced by the absorbed solar radiation is converted to electric voltage based on the Seebeck effect. To date, research aiming at maximizing the conversion efficiency of STE generators has focused

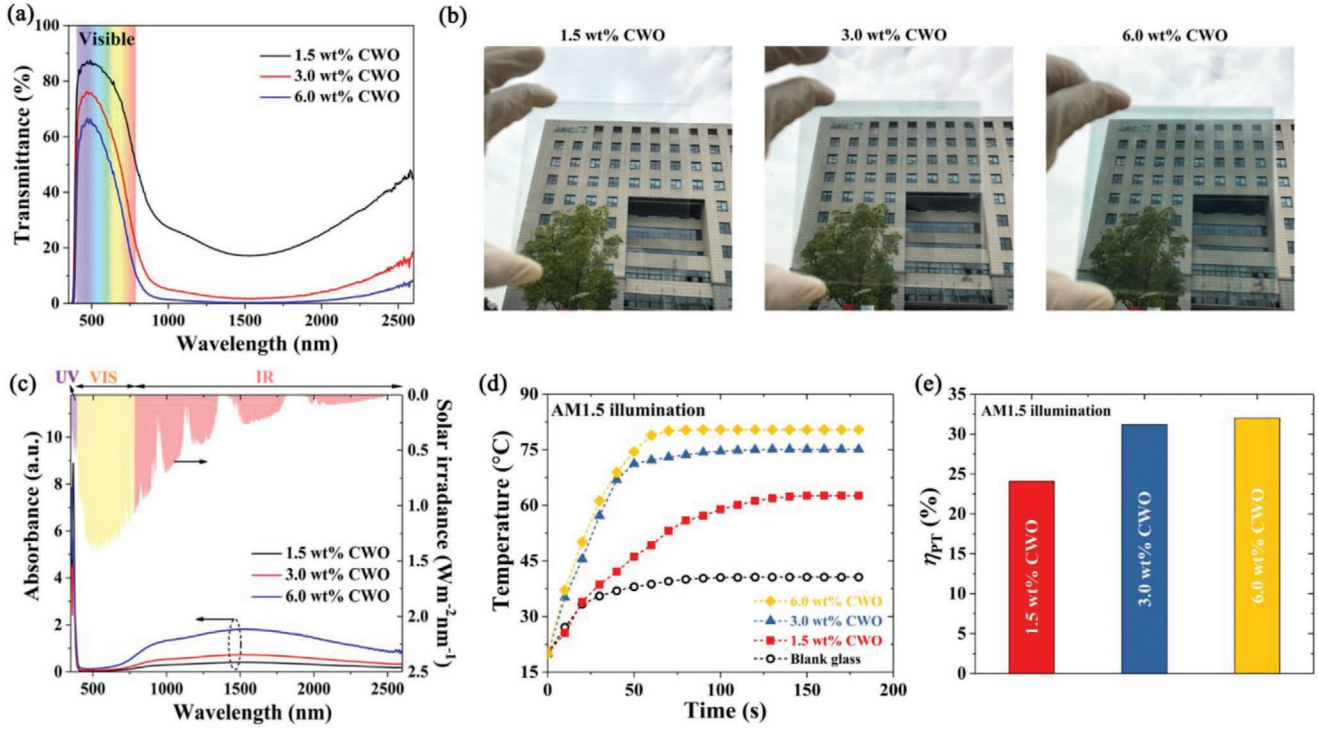

Figure 2. Physical properties of $Cs_{0.33}WO_3$ (CWO)/resin wavelength-selective films. a) Transmittance spectra of different composite films (substrate included) as a function of wavelength. b) Photographs of glass coated by the composite resin films with different weight percent (wt%) CWO, exhibiting the high transparency. c) Absorption spectra of different composite films and the solar irradiance spectrum on Earth.[23] d) Increase in temperature with time for different CWO/resin composite films under 1 sun illumination. e) Photothermal conversion efficiency (η_{PT}) of CWO/resin films.

mainly on hybrid photovoltaic-thermoelectric systems[14,17] and concentrated STE generators.[13,16] A record-high efficiency of 7.4% in concentrated STE generators was demonstrated some years ago.[16] However, despite their high performance, large-scale applications of such generators are limited by their operation in a vacuum environment and the need for high operating temperature up to 600 °C.

Here, we combine STE conversion with transparent glass to develop an efficient TPGW system with potentially widespread applicability. A film with wavelength-selective absorption is integrated onto an entirely transparent glass to allow visible light to pass through while absorbing as much ultraviolet (UV) light and near infrared (NIR) light as possible and converting them into heat (**Figure 1**a). Thermoelectric devices are designed to be attached with the film along the edge areas of the film. Heat is collected continuously by the large-area wavelength-selective film and then laterally conducted through the film to the hot side of thermoelectric devices. The glass that possesses low thermal conductivity acts as a thermal insulator to reduce the heat loss to the ambient during the lateral heat transfer process within the wavelength-selective film that covers entire area of the glass, resulting in a stable temperature difference across the thermoelectric devices. As a result, thermoelectric devices coupled with the spectrally selective film harness this heat and convert it into electricity. This power-generating system decouples the energy conversion efficiency from light transparency of the window, thus enabling independent regulation for both. Its ability to operate at ambient temperature, simple structure, and ease of installation render it suitable for widespread application.

2. Results and Discussion

2.1. Feasibility of an Improved TPGW

Studies on TPGWs have focused primarily on the wavelength-selective TPV or wavelength-selective luminescent solar concentrator (see working principle shown in Figure S1, Supporting Information). The wavelength-selective TPV uses photoactive materials to achieve high transmission of visible light and selectively absorb UV and/or NIR light. The wavelength-selective luminescent solar concentrator uses a luminescent solar concentrator with wavelength-selective luminophores that can both absorb and emit radiation outside the visible band.[1,9] However, neither method has managed to maximize the absorption of UV and NIR light. Further, both methods also inhibit the transmission of visible light because of the considerable difficulty in modifying the materials' bandgap and discontinuity of states. To overcome these limitations, we developed an approach that uses photothermal conversion, a more direct and efficient way to collect light energy.[20] We adopted an absorber that allows visible-light transmission and UV/NIR-selective absorption (Figure 1b). In combination with thermoelectric conversion, this new system is expected to simultaneously optimize transparency and power-generating performance of the system. To demonstrate the practical applicability of this approach, we connected 12 Bi_2Te_3-based thermoelectric modules in series and attached them to a 0.01 m^2 square glass piece coated by a wavelength-selective film. This power-generating system is marked by a high degree of transparency, as the objects behind the

glass are highly visible. At the same time, it can deliver a high output voltage of 3.636 V by directly harvesting sunlight from the outdoors at an ambient temperature of ≈20 °C (Figure 1c). This combination of transparency and efficiency demonstrates the feasibility and effectiveness of our approach for TPGW.

2.2. Characterizing the Performance of the Wavelength-Selective Films

Our wavelength-selective films are prepared by combining $Cs_{0.33}WO_3$ (CWO) powders with UV absorbers and resin (see the Experimental Section). The XRD pattern for CWO powders (Figure S2, Supporting Information) reveals that all diffraction peaks match well with the JCPDS data card no. 83-1334, indicating that the as-synthesized powders have a single-phase hexagonal lattice structure. Field emission scanning electron microscopy (FESEM) images reveal that the CWO powders possess near-spherical structure with the particle diameter ranging from tens to hundreds of nanometers (Figure S3, Supporting Information). Cross-sectional SEM images of the composite resin films with different weight percentages (wt%) of CWO reveal that the films are ≈10 μm thick (Figure S4, Supporting Information). Note that in our CWO/resin composite films, each sample was added with 10 wt% UV absorbers (BASF 1130 and BASF 292). From the UV–vis–NIR transmittance spectra of the CWO/resin films (**Figure 2**a), it is apparent that the films show high transmittance in the visible portion, achieving the maximum visible-light transmittance of 87.5% and an average visible-light transmittance of 84.1% (Table S1, Supporting Information). Such high optical transparency can fully meet the aesthetic requirements of window glass used in buildings and automobiles,[21]which is confirmed by viewing through the glass coated by the CWO/resin films (Figure 2b).

To use the visibly transparent composite films for generating electricity via solar-thermal-electric conversion, it is crucial to have outstanding light-selective absorption and the capability of transforming the absorbed light into heat. As is shown in the absorption spectra of Figure 2c, the CWO/resin films show a remarkable capacity to absorb UV and NIR radiation, which constitutes ≈50% of the energy of the incoming solar radiation,[22] while allowing visible light to pass through. The excellent UV absorption is attributed to the UV absorbers, while NIR absorption is facilitated by virtue of the free carrier concentration and polarons.[23]

To further evaluate the photothermal behavior of the CWO/resin composite films, we illuminated the films by using a solar simulator (standard AM 1.5 sunlight, 100 mW cm^{-2}) and monitored the temperature change. The temperature gradually increases and stabilizes. Further increasing CWO content is associated with a higher stabilized temperature, which easily reaches 80 °C for the sample with 6.0 wt% CWO/resin (Figure 2d). To quantify the photothermal conversion efficiency (η_{PT}), we adopted continuum energy balance analysis (Methods in the Supporting Information).[24,25] The 6.0 wt% CWO/resin composite exhibits η_{PT} of ≈32% (Figure 2e), of which the efficiency of converting infrared light into heat is ≈67% and efficiency of converting UV light into heat is ≈28% (Figure S5, Supporting Information). The efficiency of converting infrared light into heat is higher than that of conventional opaque photothermal materials such as Al_2O_3 (≈58%)[26] and PEDOS-C6 (≈42.5%).[27] Moreover, the CWO/resin film possesses excellent pencil scratch hardness, reaching up to 6H (Figure S6a, Supporting Information). This value is higher than that of commonly used paint films,[28] indicating its excellent abrasion resistance and robustness. In addition, when a small amount of the second phase—such as AlN nanowires and Ag nanowires—is added, the thermal conductivity of the CWO/resin films can be improved substantially (Figure S6b, Supporting Information) without affecting its optical properties (Figure S6c, Supporting Information).

Taken all together, the characteristics of high visible-light transmittance, superior light-selective absorbance, good stability, excellent mechanical property, and adjustable thermal conductivity make CWO/resin composite film a desirable candidate for transparent solar-thermal-electric (TSTE) conversion applications.

2.3. Optimized Design of STE Power-Generating Windows for Practical Application

The CWO/resin films that we developed fully meet the application requirements in terms of the transmission of visible light and achieve a high photothermal conversion efficiency. The power-generation performance of the TSTE system (see schematic in **Figure 3**a) can be improved further by optimizing the thermoelectric conversion process. For practical applications of STE power-generating windows, the wavelength-selective absorption film was designed to cover the whole window glass while thermoelectric devices were designed to be arranged along the edge areas of the glass (as illustrated in Figure 1). In such a case, heat can be collected continuously by the large-area wavelength-selective film and then is laterally conducted to the hot-side surface of thermoelectric devices, leading to the temperature increasing at the beginning and keeping the temperature stable after the system reaches the steady state. Here, we took the film temperature (T_{film}) of 75 °C as an example to optimize the device design, which is the stable temperature achieved by the 3.0 wt% CWO/resin film subjected to 1 sun illumination (Figure 2d).

We first performed the configuration design for thermoelectric devices under ideal heat-transfer conditions, in which the interfacial heat-transfer coefficients (h_h, h_c, and h_{sink}) were set as infinite. With increasing the ratio between thermoelectric leg height and total cross-sectional area (H/A_{pn}), the maximum thermoelectric conversion efficiency ($\eta_{TE,\,max}$) increases (Figure 3b) because of the increased effective temperature difference across the thermoelectric legs and the resulting open-circuit voltage (Figure S7, Supporting Information). At a certain H/A_{pn}, $\eta_{TE,max}$ reaches the peak value when the ratio of the cross-sectional areas of p- and n-type thermoelectric legs (A_p/A_n) is around 1.0, which results from the considerably matched thermoelectric material properties in this work (Figure S8, Supporting Information).[29] In addition, the $\eta_{TE,max}$ as a function of cold-side ambient temperature ($T_{ambient}$) was also calculated and is shown in Figure S9 (Supporting Information).

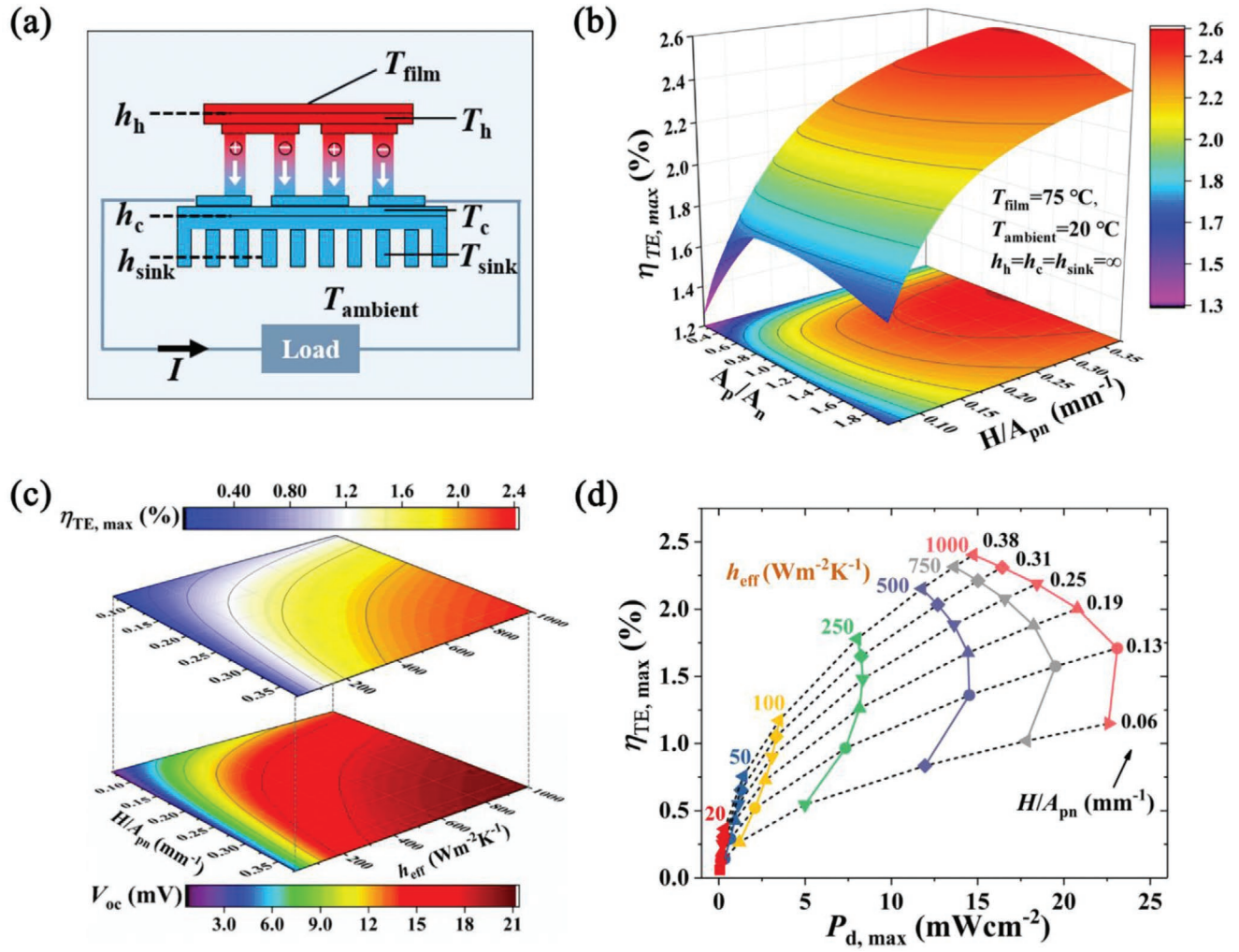

Figure 3. Numerical simulation of solar-thermal-electric power-generating windows for practical application. a) Schematics illustrating the practical solar-thermal-electric power-generating system. Temperatures (T) and convective heat transfer coefficients (h) in different parts of the system are indicated. b) 3D plots relating: 1) the maximum TE conversion efficiency ($\eta_{TE,max}$) of a unicouple; 2) the cross-sectional area ratios between p- and n-type TE legs (A_p/A_n), and ratios between height and total cross-sectional area (H/A_{pn}). c) Simulated open-circuit voltage (V_{oc}) and $\eta_{TE,max}$ under different cold-side heat transfer conditions and for different device dimensions. d) Simulated maximum TE power density ($P_{d,max}$) and $\eta_{TE,max}$ under different cold-side heat transfer conditions and for different device dimensions.

In practice, fins are usually required as the heat sink on the cold side of thermoelectric devices to augment the heat rejection (Figure 3a). The heat transfer capacity of a heat sink is a function of several parameters such as thermal conductivity of the fin material, total surface area exposed for cooling, and convection coefficient of the cooling environment. The capacity can thus vary considerably by varying any of these parameters.[30] Here, an effective heat transfer coefficient (h_{eff}) is adopted to elucidate the effect of heat sink.[31] Both open-circuit voltage (V_{oc}) and $\eta_{TE,max}$ increase with increasing H/A_{pn} and h_{eff} (Figure 3c), mainly because of the significantly increased effective temperature difference (T_h–T_c) (Figures S10 and S11, Supporting Information), which implies that larger output voltage and higher conversion efficiency can be achieved simultaneously. However, the maximum power density ($P_{d,max}$) decreases as H/A_{pn} increases under the higher h_{eff} (Figure 3d), because the increase in resistance exceeds that in voltage (Figure S12, Supporting Information). Nevertheless, both $P_{d,max}$ and $\eta_{TE,max}$ increase with increasing h_{eff} at the fixed H/A_{pn} because of the significantly increased temperature difference (T_h–T_c) (Figure S10, Supporting Information). This indicates that high $P_{d,max}$ and $\eta_{TE,max}$ can also be achieved simultaneously.

2.4. Experimental Demonstration of Solar-Thermal-Electric Power-Generating Windows

Based on the simulation results, we fabricated Bi_2Te_3-based thermoelectric modules by using the legs with high H/A_{pn} (Methods in the Supporting Information) and attached the copper radiating fins to the cold side of each module. A total of 12 modules were then fixed onto a 10 × 10 cm^2 glass that was coated with the 3.0 wt% CWO/resin film and finally connected in series (Figure S13, Supporting Information). Their

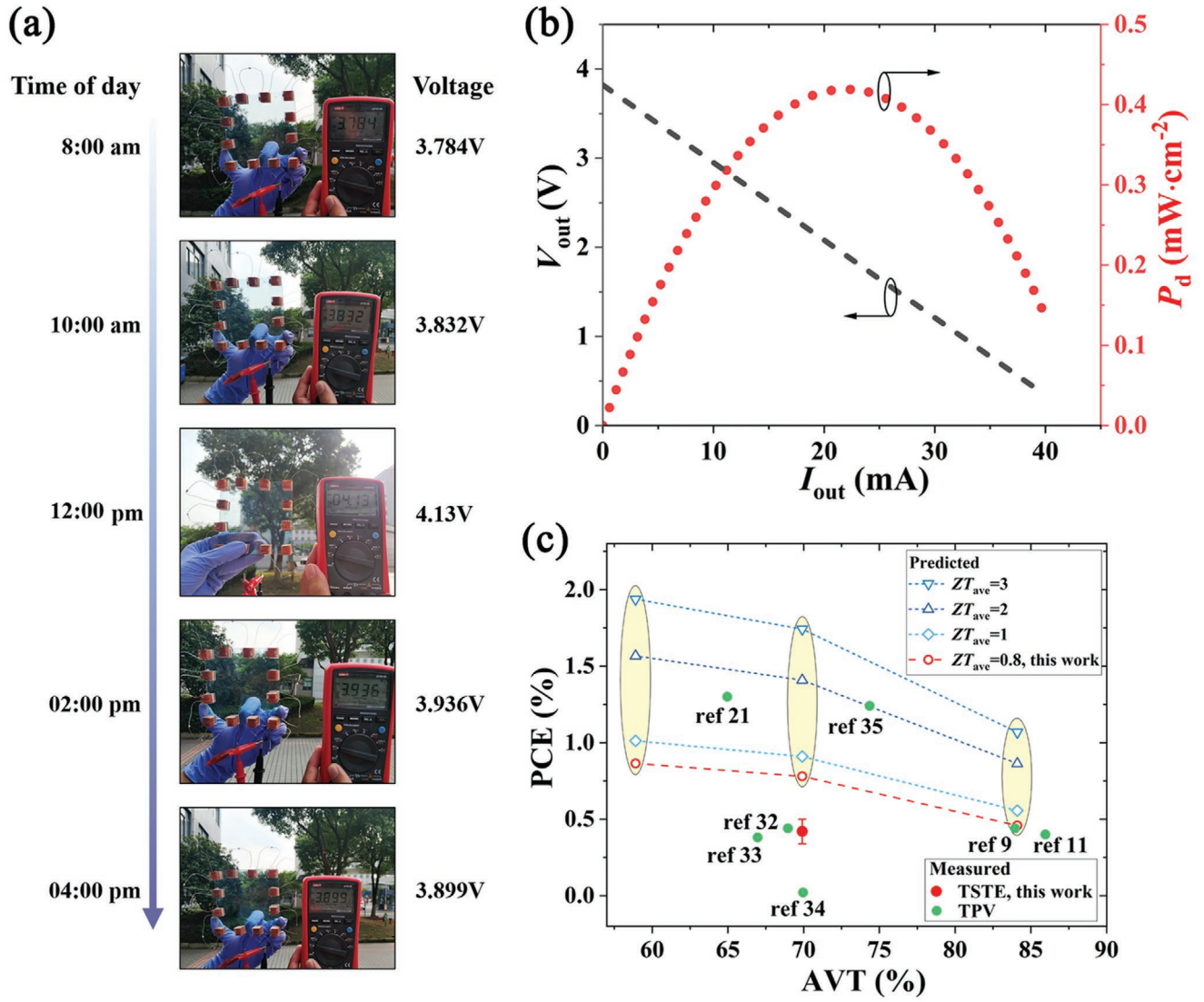

Figure 4. Power-generating performance of a typical solar-thermal-electric power-generating window. a) The window contains 12 Bi_2Te_3-based thermoelectric modules and is illuminated by outdoor sunlight at different times of the day. b) Measured current–voltage and current–power density plots of the demonstrated TSTE device. c) Measured and predicted power conversion efficiency (PCE) as a function of average visible transmission (AVT) of the TSTE device. The PCE values of some TPV technologies from literature are also plotted for comparison.[9,11,21,32–35]

power-generation performance was then characterized under the direct illumination of outdoor sunlight (**Figure 4**a and Figure S14, Supporting Information) and an indoor solar simulator (Figure S15, Supporting Information), respectively. The glass was kept perpendicular to the solar light during the measurement. For the outdoor testing, the output voltage easily reached up to ≈4 V at different times of the day (Figure 4), demonstrating a strong electric generating capacity. For the indoor testing, the current–voltage and current–power density plots under illumination of AM 1.5 sunlight (100 mW cm^{-2}) are shown in Figure 4b. The open-circuit voltage is ≈3.8 V and the maximum power density is ≈0.4 mW cm^{-2}. Following this, a thermal cycling test was conducted on the Bi_2Te_3-based thermoelectric module. Under the service condition, when the hot-side temperature was cycled between 30 and 75 °C while the cold-side temperature was held at ≈20 °C (Figure S16, Supporting Information), the open-circuit voltage, internal resistance, and output power all kept stable after 690 cycles (≈1000 h, Figure S17, Supporting Information), demonstrating excellent service performance.

As is shown in Figure 4c, when average visible transmission (AVT) (Table S1, Supporting Information) reaches 70%, the PCE of our TSTE technology is around 0.4%, which is comparable to that of reported TPV technologies.[9,11,21,32–35] Moreover, the PCE will reach up to 0.8% if ideal heat-transfer conditions are achieved with the materials used in this work. More importantly, we can independently regulate the power conversion efficiency and transparency of the window, which means that by using the thermoelectric materials with higher zT values, PCE values can be significantly enhanced without impairing AVT (Figure 4c and Figure S18, Supporting Information). Therefore, theoretically, even if the transparency exceeds 90%, extremely

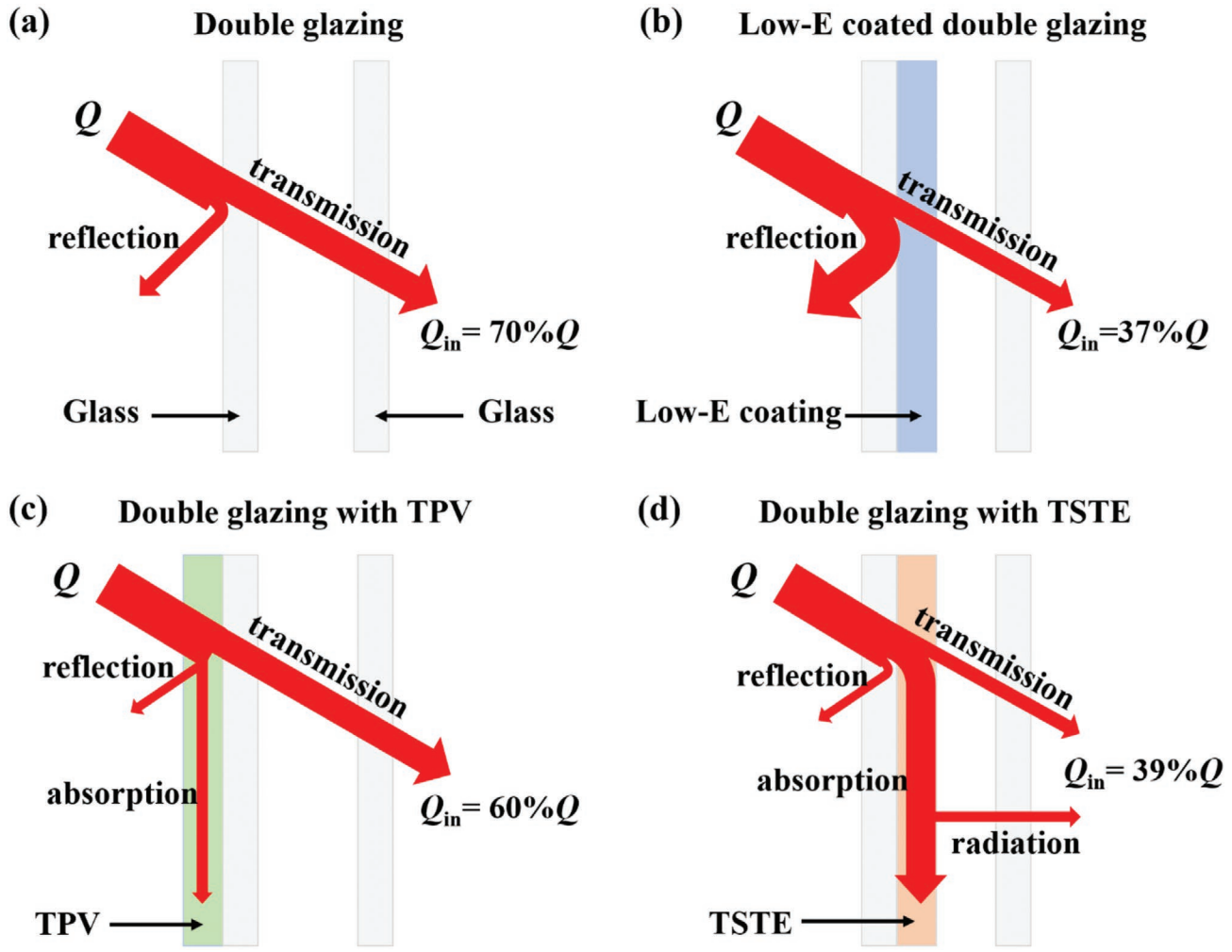

Figure 5. Simplified model showing the heat transfer process within the double pane units equipped with low-E coatings, TPV devices or TSTE devices. a) Only double glazing, b) low-E coated double glazing, c) double glazing with TPV devices, and d) double glazing with TSTE devices.

efficient power generation still can be achieved, because only the UV and IR light are used for generating the heat.

We believe that this TSTE technology will enrich the research visions of the window with energy harvesting and electricity generation,[36] as it can also be used in conjunction with TPV technology. Both technologies can complement each other as the current photovoltaic technology is typically limited to the wavelength ranging from 1100 to 1500 nm for single-junction photovoltaic cells,[1] while the wavelength-selective film expands the absorption range greater than 2500 nm, providing new option for full-spectrum utilization of solar energy. To scale up this technology, cost that impacts the practical application should be further lowered (Note S1, Supporting Information). Besides, more systematic and complete analysis from the perspective of the entire power generation system is necessary to optimize the specification and arrangement of thermoelectric modules based on analyzing the lateral heat conduction (Figures S19 and S20, Supporting Information) and minimizing the heat losses coming from convection and radiation (Note S2, Supporting Information).

2.5. Energy-Saving Analysis and Comparison

Furthermore, we estimated the heat transfer process within the double pane units to evaluate the energy-saving effects of different smart windows (**Figure 5** and Figure S21, Supporting Information). The light transmission performance of different materials used for calculating the heat transfer process is shown in Table S2 (Supporting Information). As is shown in Figure 5a, there is 70% heat that is transmitted through a clear double glazing, which is consistent with ref. [37]. In contrast, 37% of heat transfers into the indoors when a low-emissivity (low-E) coating is used (Figure 5b), because most IR light is reflected.[37,38] When a TPV device is applied (Figure 5c), around 60% of heat transfers into the indoors due to the low-efficiency utilization of infrared light in current TPV devices.[1,21,35] As for our TSTE devices in this work, the heat that transfers into the indoors consists of two parts (transmitted heat and radiant heat), as is shown in Figure 5d and Figure S21 (Supporting Information). As a result, the heat being transferred into the indoors takes up 39% of

the total input energy when the double glazing is equipped with the TSTE devices (Figure 5d) and decreases as low as 28% when double glazing with both TSTE devices and low-E coating are used (Figure S21, Supporting Information). Comparing the above energy ratio values, we can find that due to IR light being absorbed by the wavelength-selective film, our TSTE devices can significantly reduce the indoor environmental cooling load and achieve more efficient energy savings. Therefore, the TSTE technology proposed in this work has great application prospects in transparent on-site power generation and providing thermal comfort for building occupants.

3. Conclusion

We propose a new type of transparent power-generating windows that combines solar-thermal-electric conversion with materials' wavelength-selective absorption. The wavelength-selective film consisting of $Cs_{0.33}WO_3$ and resin possesses high visible-light transmittance of up to 88% and allows for efficient and selective harvesting of ultraviolet and infrared lights. Both our experiments and simulations show that this technology can, by using the photothermal and thermoelectric effects, decouple transparency from power-generation performance and enable both high output voltage and high conversion efficiency simultaneously. High AVT of 59–84% and large PCE of over 1% can be achieved by using this technology, making it a good complement with current TPVs, as TSTE conversion works well in the entire UV and NIR wavelength range, while current single-junction TPV cells work well in wavelengths lower than 1500 nm. In light of the many advantages of using CWO/resin composite films as well as the intrinsic advantages of thermoelectric power generation, this technology has great potential to be applied in the windows of all types of buildings. It provides a different working mechanism from TPVs to harvest solar energy and generate on-site electricity helping to achieve net-zero energy consumption buildings. When high transparency of window is required, TSTE technology may have great advantages compared to current TPV technology. Meanwhile, owing to UV and NIR being removed from the solar spectrum by the wavelength-selective film, this technology can also reduce cooling load for buildings in cooling-dominant climate areas, achieving efficient energy saving and transparent power generation at the same time.

4. Experimental Section

Synthesis of CWO Powders and CWO/Resin Composite Films: CWO powders were synthesized by using a previously reported method.[39] WO_3 and cesium carbonate (Cs_2CO_3) with the W and Cs elemental ratio of 1:0.33 were dissolved in deionized water and stirred for 30 min, followed by drying at 180 °C for 12 h. The mixed powders were then heated and kept at 550 °C for 1 h using a flowing H_2/N_2 gas mixture (H_2/N_2 = 25/75) in a tubular furnace. For preparing composite films, the as-synthesized CWO powders (30 wt%) were first ball-milled with polymer dispersant (10 wt%) and propylene glycol monomethyl ether acetate (PGMEA, 60 wt%) for 2 h for obtaining the CWO dispersion. Following this, silicone resin (70 wt%), UV-absorbers (BASF 1130 and BASF 292, 10 wt%), leveling agent (0.1 wt%), and polymerization inhibitor agent (1 wt%) were added to the CWO dispersion with magnetic stirring for 2 h under ambient conditions. Finally, the stable composite solution was sprayed onto the glass substrates and dried naturally.

Materials Characterization: The phase purity and crystal structure were characterized by powder XRD (Rigaku, Rint 2000, Cu Kα). The microstructures, including the morphology of CWO powders and cross section of CWO/resin composite films, were analyzed by FESEM (ZEISS SUPRA 55). The transmittance spectra and absorption spectra were evaluated at wavelengths ranging from 2600 to 350 nm on a UV–vis–NIR spectrophotometer (HITACHI, U-3010). The thermal conductivity was determined by quick thermal conductivity meter (QTM500) and the mechanical strength was tested by pencil scratch hardness test (TQC VF2377).

Device Modeling and Optimization: The simulations were performed using finite element analysis through the ANSYS-Workbench platform. The 3D models were constructed by considering the temperature-dependent materials' properties and various parasitic losses. The thermoelectric performances of bismuth telluride used in this work are shown in Figure S8 (Supporting Information). The properties of bonding materials and the contact resistances were chosen based on a previous research.[29,40] During the optimization of A_p/A_n and H/A_{pn}, A_{pn} was kept constant, following the approach detailed in ref. [41]. Important parameters such as open-circuit voltage, power density, and conversion efficiency, which are closely related to the figure-of-merit zT of thermoelectric materials, temperature difference across the device, geometric structure, and parasitic losses (Methods in the Supporting Information and ref. [29]), are evaluated. Before optimizing the design, the 3D finite element numerical simulation on a conventional Bi_2Te_3-based TE module to validate the model is conducted (Figures S22 and S23, Supporting Information).

Supporting Information

Supporting Information is available from the Wiley Online Library or from the author.

Acknowledgements

Q.H.Z. and A.B.H. contributed equally to this work. The authors gratefully acknowledge the financial support from the National Key Research and Development Program of China (No. 2019YFE0103500), National Natural Science Foundation of China (Nos. 51632010, 51902333, and 51972328), and Key Research Program of Frontier Sciences, CAS (No. ZDBS-LY-JSC037). The authors also thank Prof. Lianjun Wang and Mr. Jiancheng Wang from Donghua University for the fruitful collaborations, and Mr. Chao Wang and Dr. Shun Wan from Shanghai Institute of Ceramics for the assistance in device assembly and material measurements. Y.P.F. acknowledges the financial support from EU Marie Curie Global Fellowship (No. 841183). Q.H.Z. acknowledges the financial support from Alexander von Humboldt Foundation (No. CHN 1210297 HFST-P).

Open access funding enabled and organized by Projekt DEAL.

Conflict of Interest

The authors declare no conflict of interest.

Data Availability Statement

Research data are not shared.

Keywords

energy-saving, solar-thermal-electric conversion, thermoelectric devices, transparent power-generating windows, visible-light transmittance, wavelength-selective absorption

Received: April 16, 2021
Revised: May 28, 2021
Published online:

[1] C. J. Traverse, R. Pandey, M. C. Barr, R. R. Lunt, *Nat. Energy* **2017**, *2*, 849.
[2] Lin, M. Lai, L. Dou, C. S. Kley, H. Chen, F. Peng, J. Sun, D. Lu, S. A. Hawks, C. Xie, F. Cui, A. P. Alivisatos, D. T. Limmer, P. Yang, *Nat. Mater.* **2018**, *17*, 261.
[3] Q. Xue, R. Xia, C. J. Brabec, H.-L. Yip, *Energy Environ. Sci.* **2018**, *11*, 1688.
[4] http://data.stats.gov.cn/easyquery.htm?cn=C01&zb=A0F0P&sj=2019 (accessed: July 2020).
[5] http://www.nea.gov.cn/2020-01/20/c_138720877.htm (accessed: July 2020).
[6] N. C. Davy, M. Sezen-Edmonds, J. Gao, X. Lin, A. Liu, N. Yao, A. Kahn, Y.-L. Loo, *Nat. Energy* **2017**, *2*, 17104.
[7] R. Xia, C. J. Brabec, H.-L. Yip, Y. Cao, *Joule* **2019**, *3*, 2241.
[8] K.-S. Chen, J.-F. Salinas, H.-L. Yip, L. Huo, J. Hou, A. K. Y. Jen, *Energy Environ. Sci.* **2012**, *5*, 9551.
[9] Y. Zhao, R. R. Lunt, *Adv. Energy Mater.* **2013**, *3*, 1143.
[10] E. D. Gaspera, Y. Peng, Q. Hou, L. Spiccia, U. Bach, J. J. Jasieniak, Y.-B. Cheng, *Nano Energy* **2015**, *13*, 249.
[11] Y. Zhao, G. A. Meek, B. G. Levine, R. R. Lunt, *Adv. Opt. Mater.* **2014**, *2*, 606.
[12] D. Liu, C. Yang, R. R. Lunt, *Joule* **2018**, *2*, 1827.
[13] D. Kraemer, B. Poudel, H. P. Feng, J. C. Caylor, B. Yu, X. Yan, Y. Ma, X. Wang, D. Wang, A. Muto, K. McEnaney, M. Chiesa, Z. Ren, G. Chen, *Nat. Mater.* **2011**, *10*, 532.
[14] N. Wang, L. Han, H. He, N.-H. Park, K. Koumoto, *Energy Environ. Sci.* **2011**, *4*, 3676.
[15] L. L. Baranowski, G. J. Snyder, E. S. Toberer, *Energy Environ. Sci.* **2012**, *5*, 9055.
[16] D. Kraemer, Q. Jie, K. McEnaney, F. Cao, W. Liu, L. A. Weinstein, J. Loomis, Z. Ren, G. Chen, *Nat. Energy* **2016**, *1*, 16153.
[17] X. Su, P. Wei, H. Li, W. Liu, Y. Yan, P. Li, C. Su, C. Xie, W. Zhao, P. Zhai, Q. Zhang, X. Tang, C. Uher, *Adv. Mater.* **2017**, *29*, 1602013.
[18] J. P. Jurado, B. Dörling, O. Zapata-Arteaga, A. Roig, A. Mihi, M. Campoy-Quiles, *Adv. Energy Mater.* **2019**, *9*, 1902385.
[19] X. Lu, P. Jiang, X. Bao, *Nat. Commun.* **2019**, *10*, 138.
[20] K. T. Lin, H. Lin, T. Yang, B. Jia, *Nat. Commun.* **2020**, *11*, 1389.
[21] R. R. Lunt, V. Bulovic, *Appl. Phys. Lett.* **2011**, *98*, 113305.
[22] https://www.nrel.gov/grid/solar-resource/spectra-am1.5.html (accessed: June 2020).
[23] S. H. Hosseini, A. Azimi, M. B. Dolabi, *Mater. Res. Innov.* **2019**, *24*, 1677302.
[24] K. Wang, Y. Hou, B. Poudel, D. Yang, Y. Jiang, M. G. Kang, K. Wang, C. Wu, S. Priya, *Adv. Energy Mater.* **2019**, *9*, 1901753.
[25] H. Jin, G. Lin, L. Bai, M. Amjad, E. P. B. Filho, D. Wen, *Sol. Energy* **2016**, *139*, 278.
[26] T. Yousefi, F. Veysi, E. Shojaeizadeh, S. Zinadini, *Renewable Energy* **2012**, *39*, 293.
[27] X. Lu, L. Sun, P. Jiang, X. Bao, *Adv. Mater.* **2019**, *31*, 1902044.
[28] http://www.pencilpages.com/articles/simmons.html (accessed: July 2020).
[29] Q. Zhang, J. Liao, Y. Tang, M. Gu, C. Ming, P. Qiu, S. Bai, X. Shi, C. Uher, L. Chen, *Energy Environ. Sci.* **2017**, *10*, 956.
[30] R. A. Kishore, A. Nozariasbmarz, B. Poudel, M. Sanghadasa, S. Priya, *Nat. Commun.* **2019**, *10*, 1765.
[31] C. C. Wang, C. I. Hung, W. H. Chen, *Energy* **2012**, *39*, 236.
[32] Y. Peng, L. Zhang, N. Cheng, T. Andrew, *Energies* **2017**, *10*, 707.
[33] Aharon, M. Layani, B.-E. Cohen, E. Shukrun, S. Magdassi, L. Etgar, *Adv. Mater. Interfaces* **2015**, *2*, 1500118.
[34] M. Warasawa, Y. Watanabe, J. Ishida, Y. Murata, S. F. Chichibu, M. Sugiyama, *Jpn. J. Appl. Phys.* **2013**, *52*, 021102.
[35] C. Yang, M. Moemeni, M. Bates, W. Sheng, B. Borhan, R. R. Lunt, *Adv. Opt. Mater.* **2020**, *8*, 1901536.
[36] Y. Ke, J. Chen, G. Lin, S. Wang, Y. Zhou, J. Yin, P. S. Lee, Y. Long, *Adv. Energy Mater.* **2019**, *9*, 1902066.
[37] https://www.commercialwindows.org/lowe.php (accessed: February 2021).
[38] A. Luis, J. Hasila, V. C. Mariana, R. Saffa, *Int. J. Low-Carbon Technol.* **2020**, *15*, 112.
[39] Y. Zhou, A. Huang, H. Zhou, S. Ji, P. Jin, *Nanotechnology* **2018**, *29*, 095705.
[40] X. Lu, Q. Zhang, J. Liao, H. Chen, Y. Fan, J. Xing, S. Gu, J. Huang, J. Ma, J. Wang, L. Wang, W. Jiang, *Adv. Energy Mater.* **2019**, *10*, 1902986.
[41] Y. Xing, R. Liu, J. Liao, Q. Zhang, X. Xia, C. Wang, H. Huang, J. Chu, M. Gu, T. Zhu, C. Zhu, F. Xu, D. Yao, Y. Zeng, S. Bai, C. Uher, L. Chen, *Energy Environ. Sci.* **2019**, *12*, 3390.